Journal of Alloys and Compounds 506 (2010) 461–467

Contents lists available at ScienceDirect

Journal of Alloys and Compounds

journal homepage: www.elsevier.com/locate/jallcom

Characterization of oxide scales to evaluate high temperature oxidation behavior of Ti(C,N)-based cermets in static air

Qingqing Yang[a], Weihao Xiong[a,*], Shiqi Li[b], Hongxia Dai[a], Jun Li[a]

[a] State Key Lab of Materials Formation and Dies & Moulds Technology, Huazhong University of Science and Technology, Wuhan 430074, PR China
[b] School of Mechanical Science & Engineering, Huazhong University of Science and Technology, Wuhan 430074, PR China

ARTICLE INFO

Article history:
Received 5 November 2009
Received in revised form 2 July 2010
Accepted 7 July 2010
Available online 15 July 2010

Keywords:
Ti(C,N)-based cermets
Oxide scales
Transition layers
Oxidation behavior
High temperature

ABSTRACT

Two Ti(C,N)-based cermets with Ni and Ni–20Cr metallic binder were oxidized at 800 °C and 1000 °C for up to 100 h in static air, and the oxide scales and the transition layers formed on both the cermets were characterized to evaluate their high temperature oxidation behavior in static air using XRD, SEM and EDS. The oxide scales formed on both the cermets at 800 °C and 1000 °C were not dense, and were multi-layered, consisting of NiO outerlayer, $NiTiO_3$ interlayer and TiO_2-based innerlayer. The transition layers were present between the oxide scales and the substrates with increasing oxidation time, which consisted of Ti-based, Ni-based and Mo-based oxides. Oxidation process of both the cermets was mainly controlled by O inward thermodynamic activity, and oxidation at 1000 °C was faster than that at 800 °C. However, cermet with Ni–20Cr metallic binder was oxidized slower than cermet with Ni metallic binder, due to the richness of Cr in Ni-based binder phase and the rim phase of Ti(C,N) ceramic grains. Cr was completely oxidized to form $Cr_{0.17}Mo_{0.83}O_2$, and was incompletely oxidized to Cr-rich Ti-based oxides, leading to the decrease of O inward thermodynamic activity.

1. Introduction

Ti(C,N)-based cermets are considered as promising materials for drying cutting tools and metal hot forming tools, due to high hardness, excellent wear resistance and superior deformation resistance at high temperature, compared with WC–Co hard metals [1–5]. However, due to the low wettability between liquid Ni binder and Ti(C,N) ceramic particles, conventional Ti(C,N)–Ni or TiC–TiN–Ni cermets have such disadvantages as low toughness and thermal shock resistance, thus they are not widely used as cutting tools and metal forming tools. A few rules of thumb have been developed for a wide application of Ti(C,N)-based cermets: Mo_2C (or Mo) and WC are usually added to enhance the wettability of Ni binder on Ti(C,N) ceramic particles and inhibit Ti(C,N) ceramic grains growth, thus resulting in the improvement of mechanical properties [6–11]; Ni is partially or wholly substituted by Co to enhance the wettability between liquid metallic binder and Ti(C,N) ceramic particles and to improve strength and toughness [6,12,13]; hard ceramic particles are refined to submicron or ultrafine scale to improve mechanical properties and wear resistance [14–16]. In addition, the introduction of NbC or TaC improves hot hardness and thermal shock resistance [1,17,18]; the introduction of VC is effective to inhibit Ti(C,N) ceramic grains growth [19]; the introduction of Cr_3C_2 improves the plasticity of the rims of Ti(C,N) ceramic grains and strengthens the interface between metallic binder and Ti(C,N) ceramic grains [20]. However, a temperature rise at or near the cutting tip of cermet cutting tools can reach 600–800 °C [21] and even 800–1000 °C [22] during high speed dry semi-finishing and finishing stainless steels and carbon steels. A temperature rise of cermet tools reaches 600–870 °C during hot extruding copper, brass alloys and bronze alloys, and reaches 950–1050 °C during hot extruding cupronickel alloys. Therefore, in these applications oxidation behavior of Ti(C,N)-based cermets plays a key role determining performance and lifetime of tools.

According to available literature [23,24], Ti(C,N)-based ceramics with rather limited content of metallic binder were unstable at 900–1100 °C in air, and morphology, microstructure and composition of the oxide scales formed on ceramics were depended on ceramic compositions and oxidation temperature. In general, hard ceramic grains of Ti(C,N)-based cermets consisted of Ti(C,N) core phase and (Ti,M)(C,N) (M = W, Mo, Ta, . . .) solid solution rim phase. However, so far there is little available literature on investigation of oxide scale characteristics and oxidation behavior of Ti(C,N)-based cermets at high temperature in air [23,25]. Therefore, oxide scale characteristic and oxidation behavior of Ti(C,N)-based cermets at high temperature in air are not well understood.

Under this perspective, this present investigation aims to characterize the oxide scales and the transition layers formed on two Ti(C,N)-based cermets with Ni and Ni–20Cr metallic binder dur-

* Corresponding author. Tel.: +86 27 87556247; fax: +86 27 87556247.
E-mail address: whxiong@mail.hust.edu.cn (W. Xiong).

0925-8388/$ – see front matter © 2010 Elsevier B.V. All rights reserved.
doi:10.1016/j.jallcom.2010.07.031

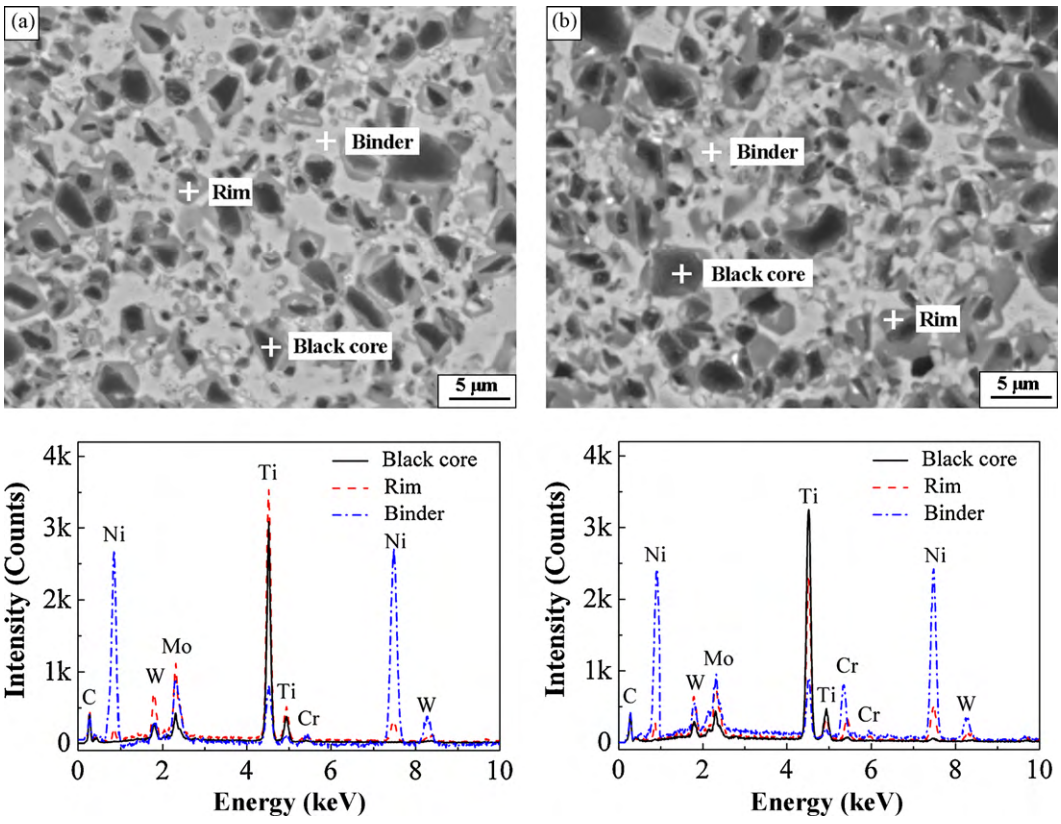

Fig. 1. SEM-BSE images and EDS spot analysis of cross-sections of cermets sintered at 1410 °C for 1 h: (a) A cermet; (b) B cermet.

ing oxidation at 800 °C and 1000 °C in static air to evaluate their high temperature oxidation behavior in static air using isothermal oxidation test, X-ray diffraction analysis (XRD), scanning electron microscopy (SEM) and energy dispersive spectrometry (EDS).

2. Experimental procedure

Commercial TiC (2.97 μm), TiN (7.30 μm), Mo (2.30 μm), WC (4.68 μm), C (<30 μm), Cr_3C_2 (2.80 μm), Ni (2.25 μm) and Cr (~74 μm) powders were used as starting powders. Two dense experimental Ti(C,N)-based cermets were prepared

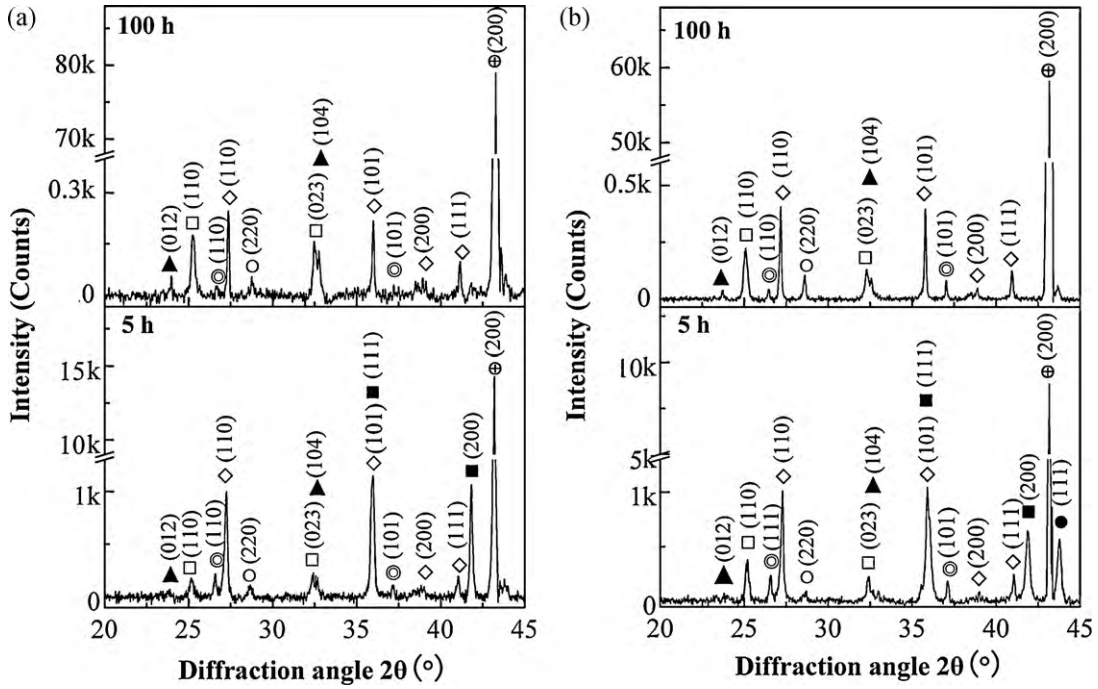

Fig. 2. XRD patterns of oxidized surface of cermets oxidized at 800 °C for 5 h and 100 h in static air: (a) A cermet; (b) B cermet (*square*, Ti(C,N); ●, Ni; ♢, TiO_2; □, Ti_3O_5; ⊕, NiO; ▲, $NiTiO_3$; ○, $NiMoO_4$; ◎, $Cr_{0.17}Mo_{0.83}O_2$).

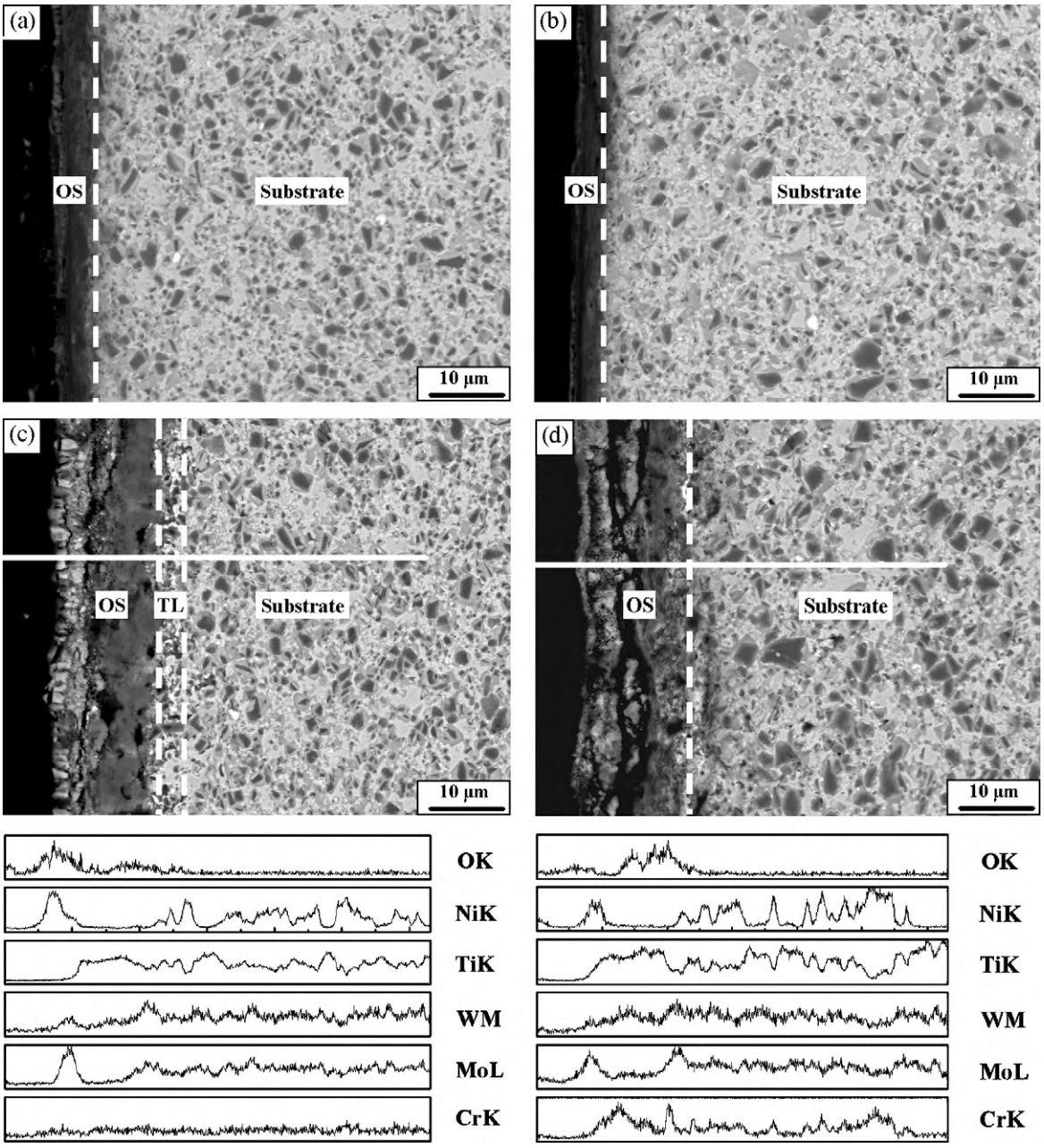

Fig. 3. Cross-section analysis of cermets after oxidation at 800 °C for different time in static air: (a) A cermet, 5 h, SEM-BSE image; (b) B cermet, 5 h, SEM-BSE image; (c) A cermet, 100 h, SEM-BSE image and EDS line analysis; (d) B cermet, 100 h, SEM-BSE image and EDS line analysis (OS, the oxide scale; TL, the transition layer).

with typical powder metallurgy technique:

A (with Ni metallic binder) :

TiC–10TiN–16Mo–6.5WC–0.8C–0.6Cr_3C_2–32Ni (wt%)

B (with Ni–20Cr metallic binder) :

TiC–10TiN–16Mo–6.5WC–0.8C–0.6Cr_3C_2–25.6Ni–6.4Cr (wt%)

The powder mixtures were planetary ball-milled using ethanol as liquid media and WC–Co hard metal balls as milling balls at a ball-to-powder weight ratio of 7:1 and a speed of 200 rpm for 48 h to obtain uniform slurry. After drying, powders were sieved, and mixed with styrene butadiene polymer, which enhanced the fluidity of powders during compaction, thus improving packing density and homogeneity of green compacts. Green compacts were pressed at the pressure of 300 MPa, and then degreased at 350–550 °C for 8 h in vacuum, and sintered at 1410 °C for 1 h in vacuum. Rockwell hardness of A and B cermets was 86.7 HRA and 89.0 HRA, respectively, and their transverse fracture strength measured by three-point bend method was 2283 MPa and 2158 MPa, respectively.

As-sintered specimens were oxidized at 800 °C and 1000 °C for different time up to 100 h in static open air in a box furnace. Before oxidation, specimens were ground up to 1000 grit SiC and polished using diamond paste with the powder sizes of W1.5 and W1, and then washed in an ultrasonic bath of acetone and dried at 120 °C. After oxidation, specimens were cooled in air out of the furnace.

Phase analysis was performed using X'Pert PRO XRD (PANalytical, Netherlands) with CuK_α radiation. Microstructure observation was performed using Quanta 200 SEM (FEI, Netherlands) in back-scattered electron (BSE) mode, and chemical composition was determined using INCA EDAX system (OXFARD, UK) attached to SEM.

3. Results

3.1. Microstructure of as-sintered Ti(C,N)-based cermets

Fig. 1 shows SEM-BSE images and EDS spot analysis of cross-sections of both the cermets sintered in vacuum at 1410 °C for 1 h. Both the cermets mainly consisted of continuous Ni-based binder skeleton and hard Ti(C,N) ceramic grains dispersed.

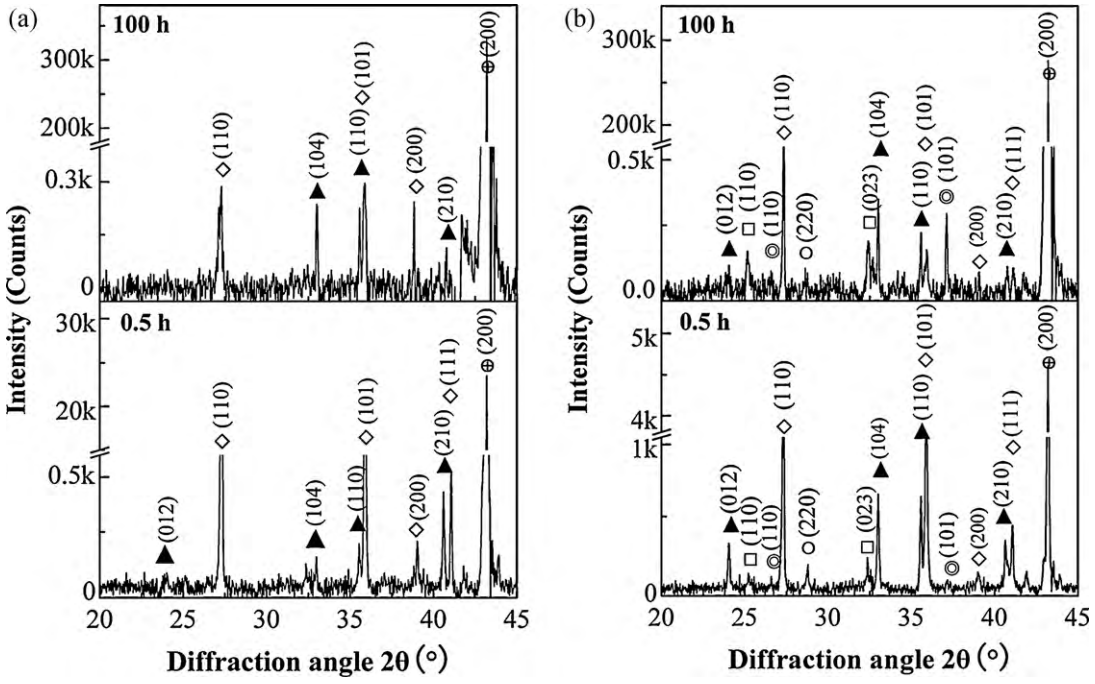

Fig. 4. XRD patterns of oxidized surfaces of cermets oxidized at 1000 °C for 0.5 h and 100 h in static air: (a) A cermet; (b) B cermet (■, Ti(C,N); ●, Ni; ♢, TiO_2; ⊕, NiO; ▲, $NiTiO_3$; ○, $NiMoO_4$; ◎, $Cr_{0.17}Mo_{0.83}O_2$).

Ti(C,N) ceramic grains in both the cermets generally exhibited a core/rim structure. The rim phase formed and grew through the dissolution–reprecipitation process around undissolved Ti(C,N) particles during liquid phase sintering [26,27]. EDS results show that Cr in both the cermets was mainly distributed in the rim phase of Ti(C,N) ceramic grains and Ni-based binder phase.

3.2. Oxide scales and transition layers formed at 800 °C in static air

Fig. 2 shows XRD patterns of oxidized surfaces of both the cermets after oxidation at 800 °C for 5 h and 100 h in static air. The oxide scale formed on both the cermets mainly consisted of crystalline NiO, TiO_2 (rutile), Ti_3O_5, $NiTiO_3$, $NiMoO_4$ and $Cr_{0.17}Mo_{0.83}O_2$.

Fig. 3 shows SEM-BSE images of cross-sections of both the cermets after oxidation at 800 °C for 5 h and 100 h in static air. After oxidation for 5 h, the thickness of the oxide scale formed was about 5 μm on A cermet and 4 μm on B cermet. After oxidation for 100 h, the thickness of the oxide scale formed was about 14 μm on A cermet and 12 μm on B cermet, and that of the transition layer formed between the oxide scale and the substrate was about 4 μm on A cermet. Fig. 3(c) and (d) shows EDS line analysis of cross-sections of both the cermets along the thickness of the oxide scales after oxidation for 100 h, respectively. Obviously, the oxide scales formed on both the cermets were multi-layered during oxidation at 800 °C, and the outerlayer contained Ni and O, the interlayer contained Ni, Ti and O, and the interlayer contained Ti and O as well as a small amount of other elements. Combined with XRD analysis of the oxidized surfaces shown in Fig. 2, the oxide scales formed on both the cermets consisted of NiO, and the interlayer consisted of $NiTiO_3$, and the innerlayer consisted of TiO_2 as well as a small amount of Ti_3O_5, $NiMoO_4$ and $Cr_{0.17}Mo_{0.83}O_2$. Morphology of the transition layer formed on A cermet was somewhat similar to that of the substrate, which was the results of incomplete oxidation of Ni-based binder and Ti(C,N) ceramic grains. EDS results demonstrated that the transition layers consisted of greywhite Ni-based oxides, and greyblack Ti-based oxides and white Mo-based oxides.

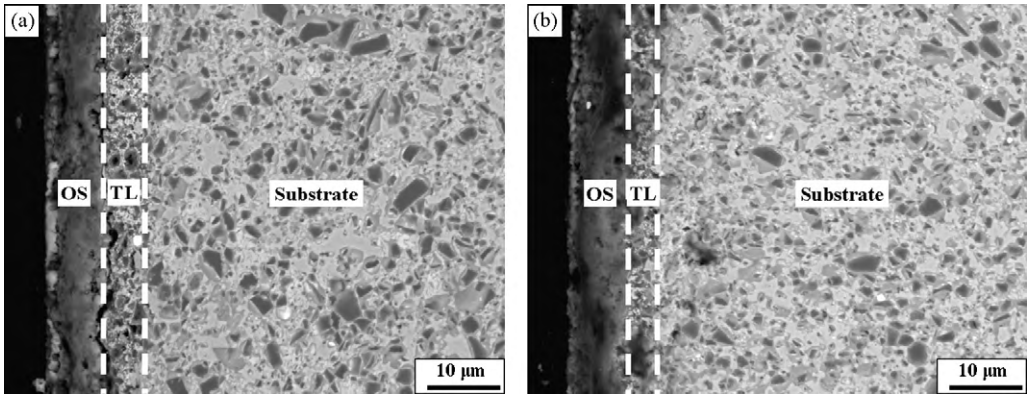

Fig. 5. SEM-BSE images of cross-sections of cermets oxidized at 1000 °C for 0.5 h in static air: (a) A cermet; (b) B cermet (OS, the oxide scale; TL, the transition layer).

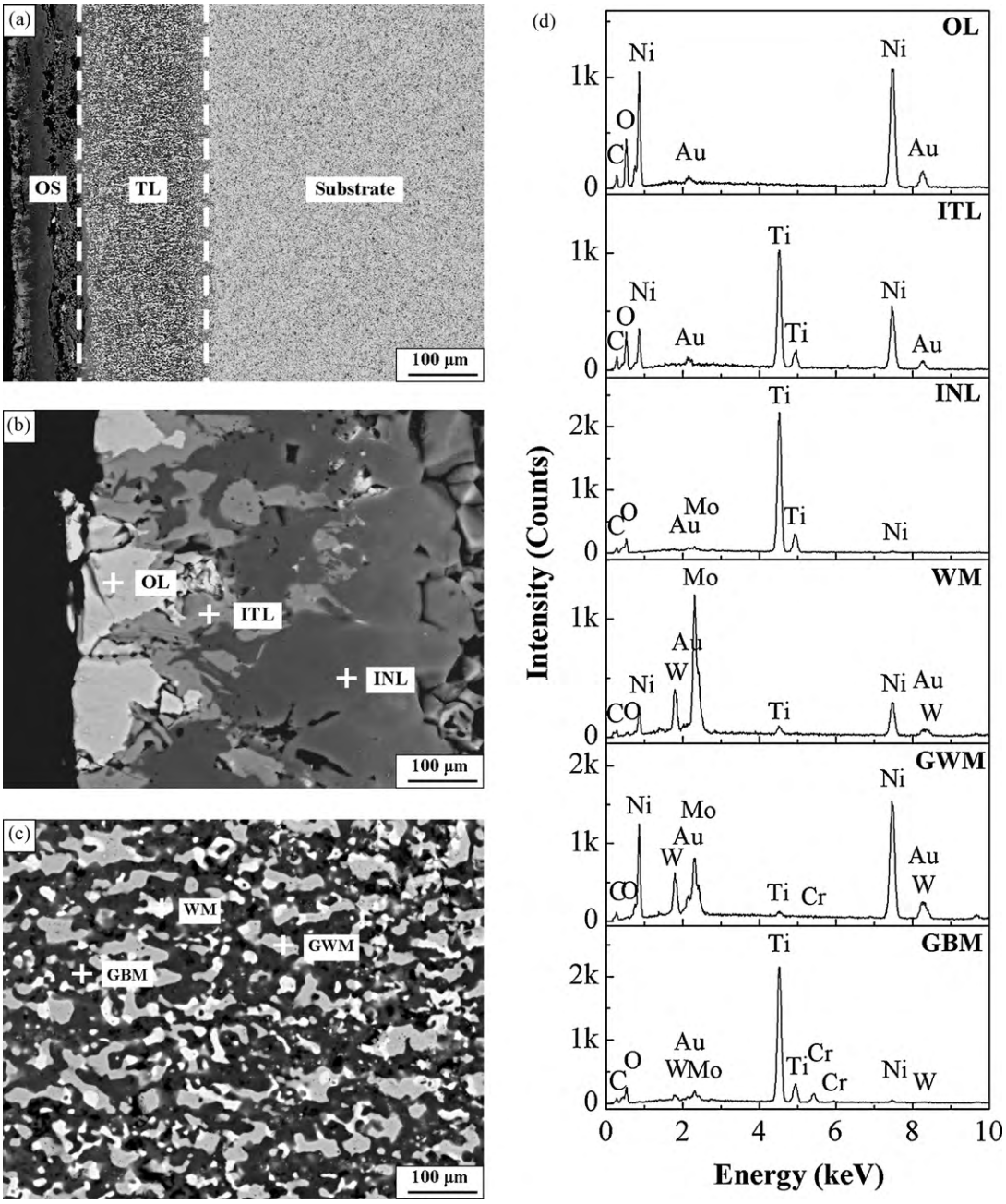

Fig. 6. Cross-section analysis of A cermet oxidized at 1000 °C for 100 h in static air: (a) SEM-BSE image of cross-section; (b) SEM-BSE image of the oxide scale; (c) SEM-BSE image of the transition layer; (d) EDS analysis corresponding to Fig. 6(b) and (c) (OS, the oxide scale; TL, the transition layer; OL, ITL and INL, the outerlayer, the interlayer and the innerlayer in the oxide scale, respectively; WM, GWM and GBM, white microstructure, greywhite microstructure and greyblack microstructure in the transition layer, respectively; Au element in EDS analysis resulting from gold plating).

3.3. Oxide scales and transition layers formed at 1000 °C in static air

Fig. 4 shows XRD patterns of oxidized surfaces of both the cermets after oxidation at 1000 °C for 0.5 h and 100 h in static air. The oxide scale formed on A cermet mainly consisted of NiO, TiO_2 and $NiTiO_3$, and that formed on B cermet mainly consisted of NiO, TiO_2, Ti_3O_5, $NiTiO_3$, $NiMoO_4$ and $Cr_{0.17}Mo_{0.83}O_2$.

Fig. 5 shows SEM-BSE images of cross-sections of both the cermets after oxidation at 1000 °C for 0.5 h in static air. After oxidation for 0.5 h, the thickness of the oxide scale formed was about 8 μm on A cermet and 7 μm on B cermet, and that of the transition layer formed was about 6 μm on A cermet and 4 μm on B cermet. Figs. 6 and 7 show SEM-BSE images and EDS spot analysis of cross-sections of A and B cermets after oxidation at 1000 °C for 100 h in static air, respectively. After oxidation for 100 h, the thickness of the oxide scale formed was about 90 μm on A cermet and 82 μm on B cermet, and that of the transition layer formed was about 175 μm on A cermet and 92 μm on B cermet. Combined with XRD analysis of the oxidized surfaces shown in Fig. 4, the oxide scales formed on both the cermets at 1000 °C were also multi-layered like those formed at 800 °C, consisting of NiO outerlayer, and $NiTiO_3$ interlayer and TiO_2-based innerlayer (containing a small amount of Ti_3O_5, $NiMoO_4$ and $Cr_{0.17}Mo_{0.83}O_2$ for B cermet). The outerlayer/interlayer and interlayer/innerlayer interfaces were fairly irregular. Morphologies of the transition layers formed on both the cermets were also somewhat similar to those of the substrates. EDS results demonstrated that the

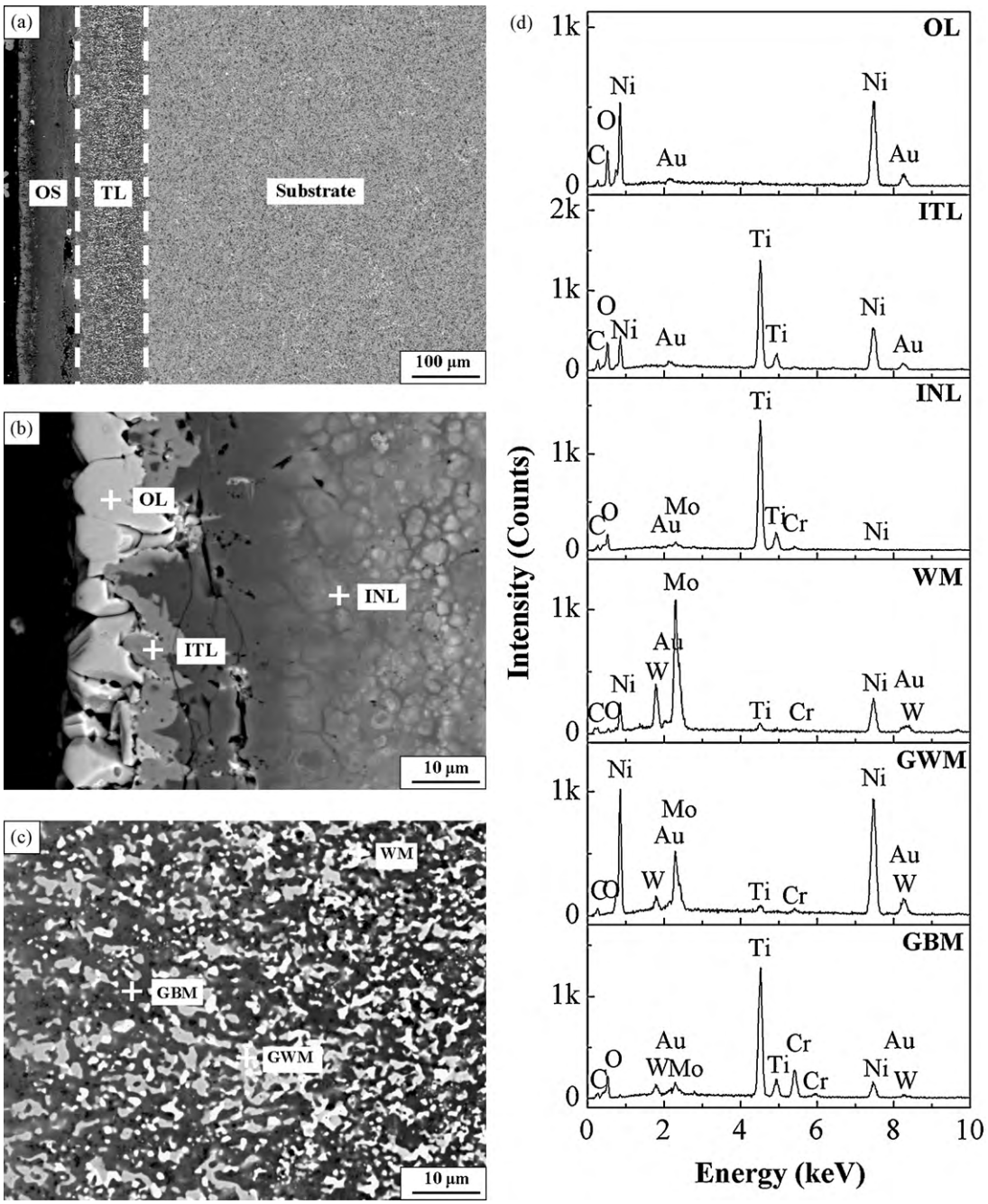

Fig. 7. Cross-section analysis of B cermet oxidized at 1000 °C for 100 h in static air: (a) SEM-BSE image of cross-section; (b) SEM-BSE image of the oxide scale; (c) SEM-BSE image of the transition layer; (d) EDS analysis corresponding to Fig. 7(b) and (c) (OS, the oxide scale; TL, the transition layer; OL, ITL and INL, the outerlayer, the interlayer and the innerlayer in the oxide scale, respectively; WM, GWM and GBM, white microstructure, greywhite microstructure and greyblack microstructure in the transition layer, respectively; Au element in EDS analysis resulting from gold plating).

transition layer formed on both the cermets at 1000 °C also consisted of Ni-based, Ti-based and Mo-based oxides. However, these oxides in the transition layer formed on B cermet were finer in morphology than those in the transition layer formed on A cermet.

4. Discussion

From the above experimental results, it can be seen that two dense experimental Ti(C,N)-based cermets with Ni and Ni–20Cr metallic binder exhibited a low thermodynamic stability at 800 °C and 1000 °C in static air, and that morphologies, microstructure and composition of the oxide scales and the transition layers formed were significantly affected by cermet composition and oxidation temperature.

For both the cermets, the oxide scales formed at 800 °C and 1000 °C mainly consisted of NiO, $NiTiO_3$ and TiO_2 (containing a small amount of Ti_3O_5, $NiMoO_4$ and $Cr_{0.17}Mo_{0.83}O_2$ for A cermet at 800 °C and for B cermet at 800 °C and 1000 °C), and the transition layers formed at 800 °C and 1000 °C consisted of Ni-based, Ti-based and Mo-based oxides (Figs. 3 and 5–7). However, the oxide scales and the transition layers formed at 800 °C grew slower than those formed at 1000 °C. After oxidation at 800 °C for 100 h, the thickness of the oxide scale was about 14 μm on A cermet and 12 μm on B cermet, and that of the transition layer was about 4 μm on A cermet, and after oxidation at 1000 °C for 100 h, the

thickness of the oxide scale was about 90 μm on A cermet and 82 μm on B cermet, and that of the transition layer was about 175 μm on A cermet and 92 μm on B cermet. Obviously, oxidation process of both the cermets was significantly controlled by oxidation temperature. During oxidation at 800 °C and 1000 °C in static air, Ni, Ti and Mo in both the cermets were completely oxidized to form crystalline NiO, crystalline TiO_2 (and a small amount of crystalline Ti_3O_5 at 800 °C for A cermet and at 800 °C and 1000 °C for B cermet) (Figs. 2 and 4) and volatile molybdenum oxides, respectively. Subsequently, NiO reacted with TiO_2 to form crystalline $NiTiO_3$, and it also reacted with molybdenum oxides to form crystalline $NiMoO_4$ at 800 °C for A cermet and at 800 °C and 1000 °C for B cermet (Figs. 2 and 4) [28]. Cr in both the cermets might be completely oxidized to form chromium oxides, which then reacted with volatile molybdenum oxides to form crystalline $Cr_{0.17}Mo_{0.83}O_2$ at 800 °C for A cermet and at 800 °C and 1000 °C for B cermet (Figs. 2 and 4). Crystalline tungsten oxides were not present in the oxide scales formed on both the cermets at 800 °C and 1000 °C (Figs. 2 and 4). This shows that W in both the cermets was completely oxidized to form volatile tungsten oxides during oxidation at 800 °C and 1000 °C. The formation of volatile tungsten oxides was verified during oxidation of Ti($C_{0.5}$,$N_{0.5}$)–16.7(WC–5Co) (wt%) ceramic and Ti($C_{0.5}$,$N_{0.5}$)–15.3(WC–5Co)–6.2Ni–2.1Co (wt%) cermet at 1000 °C in static air [23,25]. C and N in both the cermets were completely oxidized to form gaseous CO and N_2 during oxidation at 800 °C and 1000 °C, respectively [23,24]. The presence of pores and voids in the oxide scales accounted for the release of volatile tungsten oxides and molybdenum oxides, and gaseous CO and N_2 during oxidation at 800 °C and 1000 °C. With increasing oxidation time, the oxide scales became thick, and the transition layers were present between the oxide scales and the substrates as a result of incomplete oxidation. As can be seen, when the oxide scales grew, O thermodynamic activity through them into the substrates decreased so that the substrates were incompletely oxidized. When oxidation temperature increased from 800 °C to 1000 °C, O inward thermodynamic activity significantly increased, and thus oxidation of both the cermets became slow with increasing oxidation time.

Oxidation of B cermet was slower than that of A cermet, for example, after oxidation at 1000 °C for 100 h, the oxide scale and the transition layer formed on B cermet were thinner by about 8 μm and 83 μm than those formed on A cermet, respectively. This was attributed to the richness of Cr in Ni-based binder and the rims of Ti(C,N) ceramic grains (Fig. 1). Cr in Ni-based binder phase and the rim phase of Ti(C,N) ceramic grains in B cermet was completely oxidized to form $Cr_{0.17}Mo_{0.83}O_2$, and was incompletely oxidized to Cr-rich Ti-based oxides, resulting in the decrease of O inward thermodynamic activity. As a result, B cermet exhibited superior oxidation resistance at 800 °C and 1000 °C in static air.

For both the cermets, the oxide scales formed at 800 °C and 1000 °C were multi-layered, consisting of NiO outerlayer, $NiTiO_3$ interlayer and TiO_2-based innerlayer (containing a small amount of Ti_3O_5, $NiMoO_4$ and $Cr_{0.17}Mo_{0.83}O_2$ for A cermet at 800 °C and for B cermet at 800 °C and 1000 °C), and morphologies of the transition layers formed were somewhat similar to the substrates. These demonstrated that the outward diffusibility of Ni was stronger than that of Ti during oxidation at 800 °C and 1000 °C for both the cermets, and that internal oxidation process of both the cermets was mainly controlled by the interface diffusion between Ti(C,N) ceramic grains and Ni-based binder. In addition, partial spallation of the oxide scales and the presences of macrocracks and microcracks in the oxide scales and the transition layers were the result of volume contraction during air cooling from oxidation temperature to room temperature.

5. Conclusions

Two Ti(C,N)-based cermets with Ni and Ni–20Cr metallic binder (i.e. A and B cermets) were prepared with typical powder metallurgy technique and then oxidized at 800 °C and 1000 °C for up to 100 h in static air. The oxide scales and the transition layers formed were characterized to evaluate high temperature oxidation behavior of both the cermets. During oxidation at 800 °C and 1000 °C, the oxide scales formed on both the cermets were not dense, and were multi-layered, consisting of NiO outerlayer, $NiTiO_3$ interlayer and TiO_2-based innerlayer (containing a small amount of $NiMoO_4$, Ti_3O_5 and $Cr_{0.17}MoO_{0.83}O_2$ for the former cermet at 800 °C and for the latter cermet at 800 °C and 1000 °C). The transition layers formed on both the cermets at 800 °C and 1000 °C consisted of Ti-based, Ni-based and Mo-based oxides. Oxidation process was mainly controlled by O inward thermodynamic activity, and oxidation at 1000 °C was much faster than that at 800 °C. However, Ti(C,N)-based cermet with Ni–20Cr metallic binder was oxidized slower than Ti(C,N)-based cermet with Ni metallic binder, due to the richness of Cr in Ni-based binder phase and the rim phase of Ti(C,N) ceramic grains. Cr was completely oxidized to form $Cr_{0.17}Mo_{0.83}O_2$, and was incompletely oxidized to Cr-rich Ti-based oxides, leading to the decrease of O inward thermodynamic activity.

Acknowledgements

This work was funded by Natural Science Foundation of Hubei Province under Grant No. 2008CDB275 and Project of State Key Lab of Materials Formation and Dies & Moulds Technology under Grant No. 0202111011. The authors would like to thank Analytical and Testing Center at Huazhong University of Science and Technology for providing experimental facilities.

References

[1] E.B. Clark, B. Roebuck, Int. J. Refract. Met. Hard Mater. 11 (1992) 23.
[2] Y. Iyori, H. Yokoo, US patent No. 4,983,212, January 1991.
[3] H. Pastor, Mater. Sci. Eng. A 105/106 (1988) 401.
[4] H. Kolaska, Wire 40 (3) (1990) 343.
[5] D. Mari, D.R. Gonseth, Wear 165 (1993) 9.
[6] P. Ettmayer, H. Kolaska, W. Lengauer, K. Dreyer, Int. J. Refract. Met. Hard Mater. 13 (1995) 343.
[7] R. Kieffer, P. Ettmayer, M. Freudhofmeier, in: H. Hausner (Ed.), Modern Development in Powder Metallurgy, vol. 5, Plenum Press, New York, 1971, p. 201.
[8] S.Q. Zhou, W. Zhao, W.H. Xiong, Y.N. Zhou, Acta Metall. Sin. 21 (3) (2008) 211.
[9] H. Matsubars, S. Shin, T. Sskuma, Solid State Phenom. 25/26 (1992) 551.
[10] H. Suzuki, H. Matsubara, T. Saitoh, Jpn. Soc. Powder Metall. 31 (7) (1983) 236.
[11] W.T. Kwon, J.S. Park, S.W. Kim, S. Kang, Int. J. Refract. Met. Hard Mater. 44 (2004) 341.
[12] M. Ehira, A. Egami, Int. J. Refract. Met. Hard Mater. 13 (1995) 313.
[13] S. Bolognini, G. Feusier, D. Mari, T. Viatte, W. Benoit, Int. J. Refract. Met. Hard Mater. 16 (1999) 257.
[14] L.X. Yu, W.H. Xiong, P. Feng, Trans. Nonferrous Met. Soc. China 14 (3) (2004) 485.
[15] E.T. Jeon, J. Joardar, S. Kang, Int. J. Refract. Met. Hard Mater. 20 (2002) 207.
[16] J. Jung, S. Kang, J. Am. Ceram. Soc. 90 (7) (2007) 2178.
[17] F. Qi, S. Kang, Mater. Sci. Eng. A 251 (1998) 276.
[18] U. Rolander, G. Winel, M. Zwinkls, Int. J. Refract. Met. Hard Mater. 19 (2001) 325.
[19] J. Wang, Y. Liu, P. Zhang, J. Ye, M. Tu, Mater. Des. 30 (6) (2009) 2222.
[20] Y. Zheng, M. You, W.H. Xiong, W.J. Liu, S.X. Wang, J. Am. Ceram. Soc. 87 (3) (2004) 460.
[21] Y.R. Liu, J.J. Liu, B.L. Zhu, Z.B. Luo, H.Z. Miao, Wear 210 (1997) 39.
[22] X.Z. Zhao, J.J. Liu, B.L. Zhu, Z.B. Miao, Z.B. Luo, J. Mater. Sci. 32 (1997) 2963.
[23] F. Monteverde, A. Bellosi, Corros. Sci. 44 (2002) 1967.
[24] D.S. Park, C. Park, Y.D. Lee, J. Am. Ceram. Soc. 83 (3) (2000) 672.
[25] F. Monteverde, V. Medri, A. Bellosi, Mikrochim. Acta 138–139 (3–4) (2002) 97.
[26] S.Y. Ahn, S. Kang, J. Am. Ceram. Soc. 83 (6) (2000) 1489.
[27] Y. Zheng, W.H. Xiong, M. You, W.J. Liu, Trans. Nonferrous Met. Soc. China 13 (6) (2003) 1424.
[28] A. Ul-Hamid, H.M. Tawancy, A.I. Mohammed, S.S. Al-Jaroudi, N.M. Abbas, Anti-Corros. Methods Mater. 51 (5) (2004) 339.